

Experimental Validation and Extension of a BEM model for Counter Rotation Dual Rotor Wind Turbine with Double Rotational Armature Design

5 Niels Cornelis Adema^{1*}, Josep Gil-Vernet Pagonabarraga^{1,2}, Wouter Swart Ranshuysen², Arjen de Ruijter², Gerard Schepers^{1,3}

¹ Entrance - Centre of Expertise Energy part of Hanze UAS, Groningen, 9747AA, The Netherlands

² Institute of Engineering, section Mechanical Engineering, Hanze UAS, Groningen, 9747AS, The Netherlands

³ TNO Energy Transition and Materials, Delft, The Netherlands

Correspondence to: Niels C. Adema (ni.c.adema@pl.hanze.nl)

10 Abstract

Small wind turbines face significant challenges in achieving commercial viability due to lower efficiency and higher energy costs compared to utility-scale systems and competing renewable technologies. Counter-rotating dual rotor wind turbines (CR-DRWTs) with dual rotational armature configurations offer a potential pathway for efficiency improvements through doubled direct drive power and minimal mechanical complexity, suitable for urban applications. This study presents a detailed experimental investigation of a 1.6 m diameter CR-DRWT through wind tunnel testing at the Centre Scientifique et Technique du Bâtiment (CSTB) in Nantes, France, conducted at wind speeds between 4 and 15 m/s. An improved turbine design is tested with enhanced instrumentation, including independent measurements of rotor rotational speed and blade pitch angle, enabling a detailed characterization of rotor interaction, operating behaviour, and power performance. The turbine achieved a maximum electrical power output of 1014 W and a peak measured power coefficient of 0.33, while demonstrating reliable self-starting at wind speeds as low as 3.5 m/s. To interpret and generalize the experimental findings, an existing Blade Element Momentum (BEM) model for dual rotor systems is extended to explicitly represent torque balance and power production in a dual rotational armature configuration. The extended model shows good agreement with experimental trends and is further applied in a sweep optimization. The optimized configuration predicts a theoretical maximum power coefficient of 0.56, highlighting substantial remaining performance potential. By combining wind tunnel measurements with a validated BEM model extension, this work provides unique reference data and supports the development of mechanically simple CR-DRWTs for future small-scale wind energy systems.

1 Introduction

While modern wind turbines have become the largest rotating machines on earth with further upscaling planned, renewed interest in small wind turbines (SWTs) is fostered through local energy transition and smart grid development. SWTs have traditionally lacked the aerodynamic refinement of larger turbines, resulting in lower efficiency, lower capacity factors, and higher energy costs (Bianchini et al., 2022). Still, SWTs serve diverse applications worldwide, including power generation for households, industrial centres, farms, and isolated communities; hybrid energy systems for remote monitoring and telecommunications; and direct energy services like water pumping, desalination, and purification (Chagas et al., 2020). While SWTs can outperform PV systems in annual power generation at specific locations, investments require site-specific wind resource assessments, and support schemes must avoid subsidizing low-potential areas (Jurasz et al., 2025). Studies have also shown potential for urban wind applications (Bereziartua-Gonzalez et al., 2025; Calautit and Johnstone, 2023). Despite these opportunities, SWTs face significant economic challenges. Their energy costs typically exceed both residential electricity prices and those of competing technologies like rooftop solar and utility-scale wind farms. These elevated costs stem from limited development compared to large-scale systems, plus disproportionately high expenses for electrical

40 connection, resource assessment, and installation (Simic et al., 2013). To achieve commercial viability, SWTs must either achieve substantial cost reductions, for example through targeted policy incentives (Jurasz et al., 2025) or significantly improve their energy capture capability (Bianchini et al., 2022).

Dual rotor wind turbine (DRWT) configurations represent one potential pathway for efficiency gains, though this approach introduces trade-offs such as higher manufacturing costs, increased structural weight, and greater mechanical complexity.

45 DRWTs can be categorized into co-rotating systems (CO-DRWT) where both rotors rotate in the same clockwise direction or counter-rotating (CR-DRWT) systems where one rotor rotates clockwise and the other counter clockwise. Several mechanical configurations exist for dual-rotor wind turbines (DRWTs). Multiple experiments are performed on individual wind turbines placed close together or a set-up with two rotors each having a separate generator. To design a complete single DRWT system, one approach employs a bevel gear system that connects both rotors to a single generator shaft (Jung et al.,

50 2005; Schepers et al., 2024). Alternatively, a double rotational armature generator features one rotor connected to the generator stator and the other to the generator rotor (Adema et al., 2025; Booker et al., 2010; Mitulet et al., 2015). This latter configuration offers notable advantages including doubled direct drive power, minimal starting torque, high electrical and mechanical efficiency, compact design, and reduced noise and vibration—characteristics that make it particularly suitable for small-scale urban wind applications.

55 (Newman, 1986) extended the classical 1D Betz theory for single actuator discs to configurations with multiple discs demonstrating that a dual rotor system can theoretically achieve a Power Coefficient (CP) of $8/75 = 0.64$, with an induction factor of $3/5$ at the second rotor. These values exceed those of a single rotor operating at the Betz limit (CP = 0.59, induction factor = $1/3$). Through smoke visualization experiments in a wind tunnel using porous discs at varying separation distances, Newman recommended a minimum spacing of $0.5 D$ (where D is the rotor diameter) between discs to minimize flow

60 curvature and non-uniformity, thereby maintaining the validity of the 1D assumptions. More recently, (Sundararaju et al., 2017) investigated CR-DRWTs with equal-diameter rotors. They found that the maximum achievable CP reaches 0.814 when the rotors are separated by an axial distance of $2.8 D$. Their work also revealed that reducing the axial spacing toward zero causes the power coefficient to decrease progressively toward the single-rotor Betz limit.

Limited amount of field and lab scale testing on DRWTs has been performed in the past years. A field test by (Jung et al.,

65 2005) showed a CP of approximately 0.5 for a 30 kW CR-DRWT with asymmetric rotors (5.5 m front, 11 m rear) connected via bevel gears to a planetary gearbox, with simulations indicating optimal performance at $0.5 D$ spacing. Small-scale wind tunnel experiments on DRWTs are more common and have produced varying results. (Habash et al., 2011) and (Mitulet et al., 2015) both reported approximately 60% increases in energy production compared to single rotor configurations, testing turbines with rotor diameters of 23 cm and 2.5 m respectively, at spacings ranging from 0.3 - $2.3 D$ and $0.4 D$. The first using

70 individual generator per rotor and the latter a double rotational armature configuration. (Zhao et al., 2020) found relative improvements in the CP of 5.3-28.9% with a 0.55 m radius turbine at optimal $0.3 D$ spacing and individual generators per rotor. The CP values found were 0.34-0.41 versus 0.31-0.35 for single rotor operation at 8-14 m/s wind speed. A wind tunnel test including Particle Image Velocimetry (PIV) measurements comparing co- and counter-rotating DRWT systems conducted by (Ozbay et al., 2014) concluded a 60% power increase for a counter-rotating DRWT and 48% increase for a co-

75 rotating DRWT compared to a single rotor configuration. Individual turbine models with 1.27m radius at different spacings ($0.7 D$ - $6.5 D$) were tested by (Yuan et al., 2014). It was found that counter-rotating produced 20% more power compared to co-rotating in the near wake. Which decreased to only 4% at $5.0 D$. (Wang et al., 2018) tested asymmetric rotor designs (0.28 m front, 0.15 m rear, with $0.25 D$ spacing) and observed smaller gains of 7.2% for counter-rotating and 1.8% for co-rotating configurations. At $3.5 D$ (Mühle et al., 2017) found a significant improvement of 2% in power production by

80 operating the upstream rotor counter rotating.

On the contrary, no power increase was found for a bevel gear CR-DRWT system with 1.6 m rotors at $0.64 D$ spacing by (Schepers et al., 2024). But, more recently, (Adema et al., 2025) tested the same turbine with a double rotational armature

design instead of bevel gears and observed a 10% CP increase, highlighting how mechanical and electrical design may influence the observed performance of DRWT systems.

85 Modelling of DRWT systems can be categorized in two primary approaches. Blade Element Momentum (BEM) and Computational Fluid Dynamics (CFD) offer complementary insights into DRWT performance with the BEM method commonly used as the preferred tool (Peng et al., 2025). Several BEM models have been developed for DRWT systems. (Lee et al., 2012) proposed a modified BEM model for CR-DRWTs in which the rear rotor operates in the fully developed wake of the front rotor, prescribing the axial velocity deficit and neglecting tangential effects and downstream-to-upstream interactions. (Yin et al., 2022) improved physical fidelity by coupling a BE/M–T model with free-wake lifting-line data, capturing both axial and tangential inter-rotor velocity interferences, albeit with increased modelling complexity. (Amoretti et al., 2023) instead developed a configurable BEM-based approach that retains the dominant upstream wake effects while deliberately neglecting rear-to-front feedback. This offers a robust and computationally efficient framework that is particularly well suited for CR-DRWT performance prediction and parametric design studies and will be used in this study.

90 Experimental validation is crucial to increase the accuracy of these methods. Both (Amoretti et al., 2023; Yin et al., 2022) developed BEM models dedicated to DRWT systems with the first finding an increase in CP of 10.6% for a CR-DRWT with respect to single rotor and the latter a 5% CP increase. Additionally, several studies modelled DRWT systems using CFD simulations. (Wang et al., 2022) modelled a diverse range of DRWT systems using CFD-RANS (co- and counter-rotating rotors of varied sizes, including configurations with equally but also non-equally sized rotors). Compared to single rotor systems an increase in performance is found for all configurations. The benefit in performance from a counter-rotating system compared to a co-rotating system is less conclusive. A net benefit of 7% CP is found by (Rosenberg et al., 2014) using RANS by modelling the NREL 5MW rotor in combination with a 25% size secondary rotor at 0.2 D, and a 4.6% benefit using large eddy simulations. Another CFD simulation on the NREL 5MW rotor with an additional rotor of 180kW at 0.1 D downstream of the main rotor resulted in additional performance of 1.74% despite both rotors having slight efficiency decreases (Peng et al., 2025). For equal sized rotors at 0.5 D spacing a peak CP of 0.53 is found by (Koehuan et al., 2017) using CFD simulations.

Modelling of DRWT systems has furthermore received growing attention as a means to interpret experiments and explore operational parameters. Building on the work of (Amoretti et al., 2023), the present study adopts and extends their model to represent a counter-rotating DRWT equipped with a double rotational armature generator, using experimental data as the primary reference for validation and model refinement. The core contribution of this study lies in the presentation and analysis of experimental wind tunnel measurements obtained on a counter-rotating dual-rotor wind turbine tested at the Centre Scientifique et Technique du Bâtiment (CSTB) in Nantes, France, within the framework of the 2025 International Small Wind Turbine Competition. The tested turbine represents an improved design iteration of the system presented by (Adema et al., 2025) and incorporates additional instrumentation, including independent rotational speed and pitch measurements for both rotors. These measurements enable a more detailed characterization of rotor interactions, operating conditions, and power performance that has so far been scarcely documented for CR-DRWTs with double rotational armature design. In addition to reporting experimental results, the study employs an extended BEM model to interpret the measurements and to perform an operational optimization of pitch and tip-speed ratio. By grounding the modelling and optimization directly in experimental evidence, this work provides new reference data and valuable insights that support the future development and optimization of compact counter-rotating wind turbines for small-scale applications.

The remainder of the paper is structured as follows: section 2.1 presents the design of the CR-DRWT after which the wind tunnel set-up and procedure are explained in 2.2. The BEM model as well as adaptations for a double rotational armature design are shown in section 2.3. An optimization algorithm for operational parameters is laid out in section 2.4. The results of both the wind tunnel test, BEM model, and optimization are in section 3 after which the results are discussed in section 4.

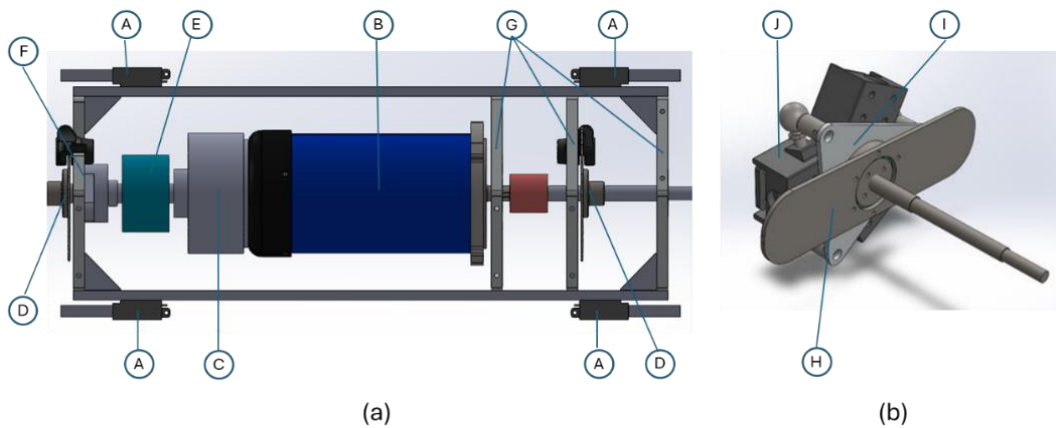
125 Conclusions are presented in section 5.

2 Methods and Materials

This chapter describes the method and materials used in the study. The mechanical, electrical, and aerodynamic design of the CR-DWT are presented after which the test procedure in the wind tunnel is explained. The BEM model used is explained including proposed extensions to model a dual rotational armature design. Finally, an optimization strategy is presented to determine optimal operating conditions for future designs.

2.1 Design of the CR-DRWT

The mechanical, electrical, and aerodynamic design of the CR-DRWT used in this study are presented in earlier work in a different wind tunnel (Adema et al., 2025). The mechanical and electrical design of the current turbine are identical as in the earlier work. The generator is still an inline Windstream 1.4 kW PMDC with operating conditions: 0-120 V, maximum current 20A for 30 minutes, 10 A continuous operation, and startup torque of 0.153 Nm. The overall efficiency of the generator in the contest conditions has been determined in previous work to be 70-90% (Adema et al., 2025; Jansma, 2024). An overview of the mechanical design including the blade pitching mechanism and blade mounts is shown in Fig. 1. Some significant changes have been made to the aerodynamic design as well as to the sensors on the turbine.



140 **Figure 1: Overview of the mechanical lay-out of the CR-DRWT. (a) Nacelle Overview, (b) Pitch Mechanism.**
(In which A: Linear Actuators, B: Generator, C: Generator Cap, D: Disc Brakes, E: Slip Ring, F: Plate with external bearing, G:
145 Plates with internal bearing, H: Push/Pull Plate, I: Triangular Place, J: Blade Holders.) Taken from (Adema et al., 2025).

Numerous studies emphasize the importance of measuring blade pitch angles and rotor RPM during wind tunnel measurements of wind turbines (Adema et al., 2025; Amoretti et al., 2023; Bai et al., 2023; Bontempo and Manna, 2025; Erturk et al., 2018; Zhao et al., 2020). Thereto, additional sensors measuring RPM and pitch angles are mounted on the CR-DRWT. Rotor RPM is measured with light pulses passing through slotted discs connected to the rotor and stator and measured by two calibrated light gate sensors. During testing only the upstream rotor RPM measurement was functional. Pitch angles are set with 4 Actuonix Motion P16-R linear actuators controlled by an Arduino Mega board with two L298B motor drivers. An Arduino-based control system is used to operate pitch and brake actuators while the generator output is monitored in real-time through a Python based data acquisition interface.

The initial pitch angle for the mounting system for the blades is changed slightly and therefore the twist distribution at zero pitch changes. The corresponding chord and twist distribution are shown in Fig. 2 alongside a zoom on the root section of the blade and connection to the blade holders. The blades consist of SG6043 airfoils and are fabricated with a 3d printed core laminated with 2 carbon fibre layers. For simplicity, the downstream rotor is mirrored with respect to the upstream rotor. The distance between rotors is fixed at 0.64 m (0.39 D) for this CR-DRWT. Rotor diameter for both rotors is 1.6 m leading to a 2 m² swept frontal area.

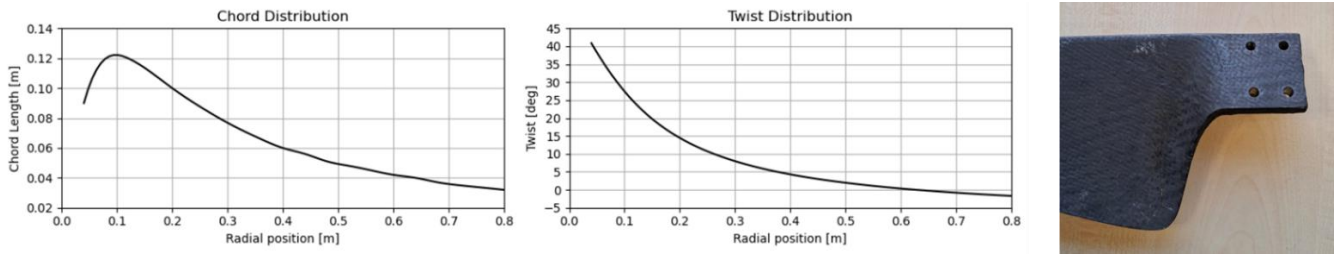


Figure 2: Aerodynamic design of both rotors of the DRWT. Left: the chord distribution. Middle: the twist distribution. Right: Zoom in on the root section of the blades.

160 **2.2 Wind Tunnel Set-up and Test Procedure**

The CR-DRWT is tested in the aerodynamic test section at CSTB. The section is 12 m long, 6 m wide, and has a height of 5 m. The airflow is controlled to keep a uniform and constant velocity, taking into consideration air density variations. The maximum free stream windspeed is 70 m/s. Turbulence intensity in the empty test section is less than 1.5% (Braud et al., 2024). The blockage ratio of the 2 m² rotor is 6.7%, which is below 10% mentioned in the literature above where corrections
 165 need to be made (Al-Obaidi and Madivaanan, 2022; Chen and Liou, 2011; Jeong et al., 2018).

The CR-DRWT is placed on steel frame connected to the floor of the wind tunnel, see Fig. 3. For mounting, testing, and dismantling of the turbines a timeslot of 2 hours was available. Wind speeds were increased in 1 m/s increments from the moment the turbine self started, starting at 4 m/s up to a maximum of 15 m/s. The DC generator is connected to a programmable Chroma DC load. The resistance of the programmable load is increased at each wind speed until the
 170 maximum power point is found. The resistance, voltage, current, and power production are measured for 10 seconds with 0.1 second intervals. From the 100 datapoints per wind speed, average values and standard deviations are determined. The measured average power is then combined with the tunnel speed, air density, and the rotor surface area to determine the power coefficient (CP) of the wind turbine.



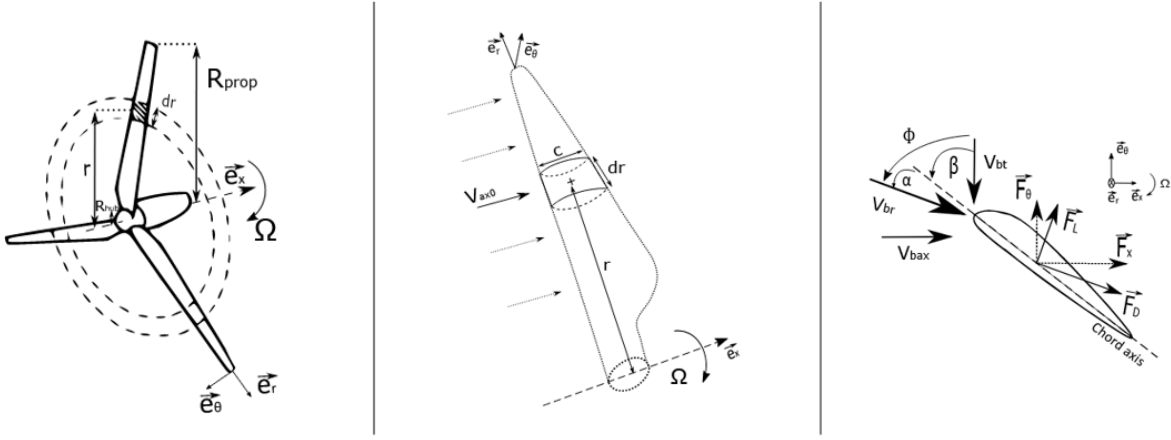
175 **Figure 3: The CR-DRWT in the wind tunnel at CSTB.**

2.3 BEM Model for Dual Rotational Armature

The BEM model in this study is based on the work of (Amoretti et al., 2023) who developed a configurable BEM model for dual rotor systems with two distinct rotors with individual generators. The present work extends this model as in a dual
 180 rotational armature configuration both rotors are connected through a single generator. The model has the following assumptions: The flow is considered inviscid and incompressible, the system is in a stationary state, the retroaction from the second rotor to the first one is neglected, there is no radial speed taken into account, the expansion of the flow at the rear of the first rotor is not considered. The last assumption is made because the expansion of two adjacent concentric annular sections would result in the intersection of the two respective flows and give complex flow velocity calculations (Amoretti et
 185 al., 2023). The model and the proposed extensions to it are presented in the following sections.

2.3.1 Single Rotor BEM

For this study, the definition of rotor, blade, and blade elements is according to Fig 4. A rotor with radius R_{rotor} and hub radius R_{hub} rotates at angular velocity Ω about the axial direction \vec{e}_x . Each blade is discretised into N elements of length dr at radial position r , characterized by chord length c , twist angle β , and the aerodynamic profile.



190

Figure 4: BEM parameters definition. Left: global wind turbine, middle: Blade element definition, right: flow velocities and forces seen by a blade element. Adapted from figures 2 to 4 from (Amoretti et al., 2023).

The axial and tangential forces on a blade element are then as in Eq. (1) and Eq. (2):

$$dF_x = \frac{1}{2} * \rho * c * dr * V_{br}^2 * [C_L * \cos(\Phi) + C_D * \sin(\Phi)] , \quad (1)$$

$$195 \quad dF_\theta = \frac{1}{2} * \rho * c * dr * V_{br}^2 * [C_L * \sin(\Phi) - C_D * \cos(\Phi)] , \quad (2)$$

Where ρ is the air density, V_{br} is the relative velocity seen by the blade, C_L and C_D are airfoil lift and drag coefficients, and Φ is the sum of angle of attack α , pitch angle, and twist angle β . The torque produced by a blade element is described as Eq. (3) leading to a total rotor power as in Eq. (4) in which B is the number of blades of the turbine. The power coefficient (C_p) can be determined as in Eq. (5) where V_{ax0} is the upstream wind speed.

$$200 \quad dM = r * dF_\theta , \quad (3)$$

$$P_{turbine} = B * \int_{R_{rotor}}^{R_{hub}} \Omega * dM , \quad (4)$$

$$C_p = \frac{P_{turbine}}{P_{wind}} = \frac{P_{turbine}}{[\frac{1}{2} * \rho * \pi * R_{rotor}^2 * V_{ax0}^3]} , \quad (5)$$

The axial and tangential velocities seen by the blade are modified by induction coefficients a and a' leading to the relative velocity following Eq. (8).

$$205 \quad V_{bax} = (1 - a) * V_{ax0} , \quad (6)$$

$$V_{bt} = (1 + a') * \Omega * r , \quad (7)$$

$$V_{br} = \sqrt{V_{bax}^2 + V_{bt}^2} \quad (8)$$

The induction coefficients are computed iteratively via a fixed-point algorithm presented in (Amoretti et al., 2023) and for each iteration the coefficient are calculated using Eq. (9) and Eq. (10). The iterative convergence criterion is set to $\varepsilon = 10^{-3}$.

$$210 \quad a_{(n+1)} = \frac{1}{\frac{4 * F * \sin(\Phi)^2}{s * [C_L * \cos(\Phi) + C_D * \sin(\Phi)]^{-1}}} , \quad (9)$$

$$a'_{(n+1)} = \frac{1}{\frac{4 * F * \sin(\Phi) * \cos(\Phi)}{s * [C_L * \sin(\Phi) - C_D * \cos(\Phi)]^{-1}}}, \quad (10)$$

In which s is the local solidity shown in Eq. (11) and F is Prandtl's tip loss factor (Hansen, 2015) as in Eq. (12) and Eq. (13):

$$s = \frac{c * B}{2 * \pi * r}, \quad (11)$$

$$F = \frac{2}{\pi} * \arccos(e^{-f}), \quad (12)$$

$$215 \quad f = \frac{B}{2} * \frac{R_{rotor} - r}{r * \sin(\Phi)}, \quad (13)$$

For high induction factors ($a > 0.2$), Spera's correction is applied (Hansen, 2015) and Eq. (9) is replaced by:

$$a_{(n+1)} = \frac{1}{2} * [2 + K * (1 - 2a) - \sqrt{(K(1 - 2a) + 2)^2 + 4(K * a^2 - 1)}], \quad (14)$$

With

$$K = \frac{4 * F * \sin(\Phi)^2}{s * [C_L * \cos(\Phi) + C_D * \sin(\Phi)]}, \quad (15)$$

220 2.3.2 Wake Velocity Evolution

For the second rotor the axial and tangential velocities downstream of the upstream rotor evolve with the distance after the rotor. The velocity evolution is defined with a distance coefficient $C_{distance}(x)$ based on propeller stages (Gur, 2019), in which x is the distance from the first rotor.

$$C_{distance}(x) = 1 + \frac{x}{\sqrt{x^2 + R_{rotor}^2}}, \quad (16)$$

225 The wake velocities at distance x from the rotor are then calculated as:

$$V_{ax}(x) = V_{ax_0} * (1 - C_{distance}(x) * a), \quad (17)$$

$$V_t(x) = -a' * \Omega * r * C_{distance}(x), \quad (18)$$

2.3.3 Dual-Rotor Configuration

For the second rotor at distance $x = d$ downstream from the upstream rotor, the upstream wind velocities are now $V_{ax}(d)$ and $V_t(d)$. The axial velocity seen by the second rotor blade is calculated in Eq. (19). The tangential velocity depends on rotation direction. In this case the counter-rotating configuration and thus following Eq. (20).

$$V_{bax2} = (1 - a_2) * V_{ax}(d), \quad (19)$$

$$V_{bt2} = (1 + a'_2) * (\Omega_2 * r - V_t(d)), \quad (20)$$

235 The BEM algorithm is applied to both rotors sequentially, with the downwind rotor calculation incorporating modified inflow conditions. All other BEM equations (forces, induction factors, corrections) remain structurally identical for the second rotor. The model accepts geometrical parameters (blade geometry, rotor radii, number of blades), aerodynamic data (lift/drag polars), operational parameters (rotational speeds), environmental conditions (wind speed, air density), and configuration settings (rotor spacing, rotation direction).

2.3.4 Extension to the model for Dual Rotational Armature Design

240 In order for a CR-DRWT with a dual rotational armature design to be in balance both rotor torques need to be equal (Kutt et al., 2020; Li et al., 2021). For a range of prescribed tip speed ratios of the upstream rotor, valid operating tip speed ratios of the downstream rotor are determined by enforcing a torque balance condition under the wake induced by the upstream rotor. The procedure used to determine these torque-balanced operating points is described in Table 1.

245

Table 1: Algorithm to determine balance torque of CR-DRWT

Algorithm Torque Balance CR-DRWT:

for each wind speed:*for each* prescribed front rotor tip speed ratio:

Compute the aerodynamic torque and rotational speed of the upstream rotor

Compute the wake conditions at the downstream rotor plane induced by the upstream rotor

Fix the wake conditions and evaluate the downstream rotor torque over a predefined range of rear rotor tip speed ratios

Identify all intervals where the downstream rotor torque crosses the upstream rotor torque

for each identified sign change interval:

Apply bisection to find the downstream rotor tip speed ratio at which both torques are balanced

Compute the downstream rotor rotational speed and power output.

Compute the total system power.

Store the torque balanced operating point.

*end for**end for**end for*

Output: Torque balanced operating points and power values for all wind speeds

The output is a list of operating points where the system is in balance according to Eq. (22). Throughout the algorithm from Table 1 a tolerance for torque balance is given of 0.05 Nm in order to find possible solutions. For each point of balance, the net generator RPM is the sum of the RPM of both rotors as the system is counter-rotating as shown in Eq. (21). The power then follows Eq. (23) and the power coefficient of the CR-DRWT is according to Eq. (24), where P_{wind} is calculated as in Eq. (5).

$$\Omega_{generator} = \Omega_{upstream\ rotor} + \Omega_{downstream\ rotor} , \quad (21)$$

$$T_{CR-DRWT} = T_{upstream\ rotor} = T_{downstream\ rotor} , \quad (22)$$

$$P_{CR-DRWT} = (\Omega_{generator} * T_{CR-DRWT}) , \quad (23)$$

$$C_{p_total} = \frac{P_{CR-DRWT}}{P_{wind}} , \quad (24)$$

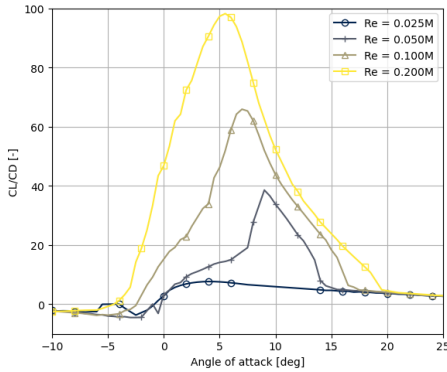
2.5 Optimization of extended CR-DRWT BEM model

The ISWTC competition of 2025 included a Weibull distribution ($A = 7.1$ and $k = 2.4$) to calculate the Annual Energy Production (AEP). Thereto, the turbine is optimized for performance in these conditions. A sweep optimization strategy to identify the pitch angle combination that maximizes the Annual Energy Production (AEP) of the dual-rotor wind turbine is employed. The upstream and downstream rotor pitch angles are each varied independently across a grid from 0° to 10° in steps of 1° , yielding 121 unique pitch combinations to be evaluated in full. For each combination, the aerodynamic performance is computed across a range of wind speeds from 4 to 15 m/s with 1 m/s interval using the extended BEM model. For each wind speed only the operating point yielding the highest overall power output is selected. The AEP for each pitch combination is then calculated using the Weibull parameters. The pitch combination producing the highest total AEP across all wind speeds is then identified as the global optimum. Finally, the BEM will then be simulated with the theoretically optimal pitch and TSR settings to assess the maximum performance of the CR-DRWT. This will then be compared to the wind tunnel measurements as well.

This chapter present the results of the wind tunnel test and BEM model including optimization. First the results of the wind tunnel are presented together with the BEM model validation.

3.1 Airfoil data

The aerodynamic data to describe the airfoil performances was generated with the 2D airfoil solver XFOIL in QBlade (QBlade - Next Generation Wind Turbine Simulation, 2026; Drela, 1989). Lift and drag coefficients for angles of attack from -10° to 25° are calculated with a transition amplification ratio of $N_{crit} = 9$ corresponding to clean wind tunnel conditions. Figure 5 displays the aerodynamic data. The curve is then extrapolated to 360° (Montgomerie, 2004). For the BEM code, the aerodynamic data is interpolated according to the individual Reynolds number for each blade element.



280 **Figure 5: Profile aerodynamics of SG6043 airfoil at $N_{crit} = 9$.**

3.2 Wind tunnel test

Air pressure in the wind tunnel at the time of the experiment was 1018 hPa, average humidity was 51.2%, and average temperature was 25.5 degrees Celsius. The density is then calculated as 1.18 kg/m^3 . The wind tunnel speed is determined through the measurement of the dynamic pressure and air density. Rotor RPM was measured in 10 RPM increments. The data was acquired through a laptop interface connected with the turbine, measurements were sampled at discrete wind speed intervals rather than continuously logged due to the streaming nature of the sensor output. The generator RPM is determined through the voltage and current measurements as well as the generator characteristics. At 6 m/s optimal operational pitch settings were determined by manually changing pitch angles and resistance values of the DC load to reach maximum power production. The settings for the collective pitch angles were 8.6 degrees for the upstream rotor and 1.7 degrees for the downstream rotor throughout the experiment. The results for the wind tunnel test are presented in Table 2. The turbine self-starts around 3.5 m/s and starts producing power at 4 m/s. A start-up procedure is developed where the downstream rotor is allowed to operate first by breaking the upstream rotor, and consecutively allowing the upstream rotor to start only once the downwind rotor reached an operating point. Power, voltage, and current output is measured for 10 seconds with 0.1 s sampling rate. Mean values are calculated as well as the standard deviation. Maximum power production was 1013.79 ± 8.58 W at 15.00 m/s wind tunnel speed. The maximum RPM of the generator was 2150 RPM. The rear rotor was generally rotating slower than the front rotor at lower wind speeds while at higher wind speeds the RPM became more similar for both rotors and the rear rotor seemed to stabilize. Net generator RPM did keep increasing with wind speed.

A simulation using the BEM code from section 2.3 with identical inputs for pitch during the experiment has been performed. The corresponding pair of rotational speeds where torque balance is present and which are closest in power output to the measurement are selected. The results for the power production, the CP, and RPMs are shown in Fig. 6, Fig. 7, and Fig. 8 together with the CSTB wind tunnel results. The BEM code imposes a 70-90% electrical efficiency of the generator on the aerodynamic power. This efficiency of the generator has been determined for similar operational conditions in previous

studies (Adema et al., 2025; Jansma, 2024). The CP values for the downstream rotor are calculated with the reduced windspeed after the upstream rotor following Eq. (17).

305 Overall, the BEM model follows the outcome of the wind tunnel tests well with respect to power output and CP values. Both rotors are operating at similar CP values. However, the modelled RPM values start to deviate from around 11 m/s onwards. The measurements show a stable upstream rotor RPM of 1050, but the model requires a faster rotating upstream rotor to enforce torque balance at that power point. The model however does follow the operational RPM of the generator indicating that the inferred RPM from the generator characteristic were correct. The discussion in the next section further elaborates on
 310 the observed deviation in RPM measurement.

Table 2: Measurement results from CSTB wind tunnel tests

Wind tunnel speed [m/s]	Voltage [V]	Current [A]	Power [W]	CP [-]	Downstream Rotor [RPM]	Upstream Rotor [RPM]	Generator [RPM]
4.14	22.71 ± 0.54	0.42 ± 0.01	9.49 ± 1.63	0.11 ± 0.02	60	340	400
5.27	31.57 ± 0.33	1.05 ± 0.01	33.31 ± 4.00	0.19 ± 0.02	260	390	650
5.90	39.38 ± 0.29	1.43 ± 0.03	56.33 ± 1.61	0.23 ± 0.01	250	540	790
7.10	38.38 ± 0.05	3.48 ± 0.01	133.58 ± 1.27	0.32 ± 0.00	210	630	840
8.16	41.75 ± 0.22	5.01 ± 0.02	209.25 ± 1.99	0.33 ± 0.00	245	705	950
9.14	49.86 ± 0.22	6.04 ± 0.01	301.05 ± 2.20	0.33 ± 0.00	360	830	1190
10.05	57.54 ± 0.19	6.97 ± 0.01	401.31 ± 1.50	0.33 ± 0.00	400	940	1340
11.15	66.45 ± 0.15	8.07 ± 0.05	535.91 ± 3.40	0.33 ± 0.00	520	1000	1520
12.18	73.51 ± 0.23	8.91 ± 0.07	654.75 ± 5.59	0.31 ± 0.00	620	1050	1670
13.04	80.12 ± 0.22	9.74 ± 0.07	780.29 ± 5.54	0.30 ± 0.00	800	1050	1850
13.93	85.91 ± 0.32	10.37 ± 0.08	890.98 ± 5.54	0.28 ± 0.00	960	1050	2010
15.00	91.72 ± 0.31	11.05 ± 0.07	1013.79 ± 8.58	0.25 ± 0.00	1100	1050	2150

315

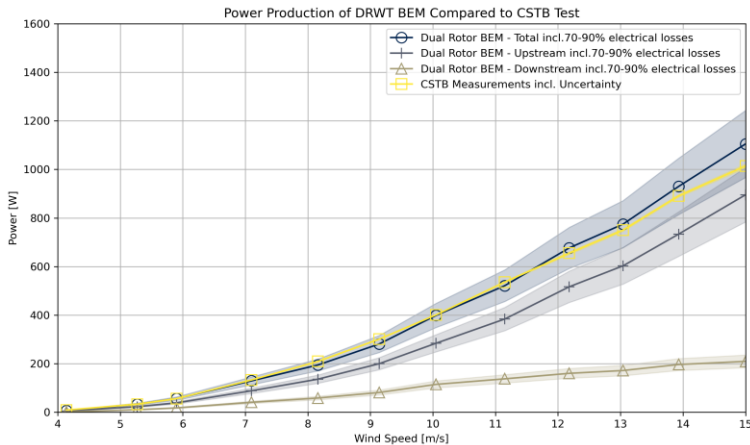
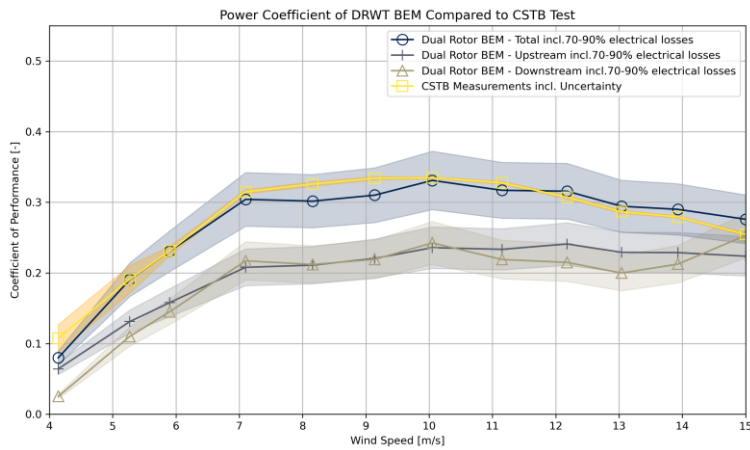


Figure 6: Results of power production during the wind tunnel test compared to BEM results. The figure shows both rotors individually, the CR-DRWT and the wind tunnel test data.



320 **Figure 7: Results of the coefficient of performance during the wind tunnel test compared to BEM results. The figure shows both rotors individually, the CR-DRWT and the wind tunnel test data.**

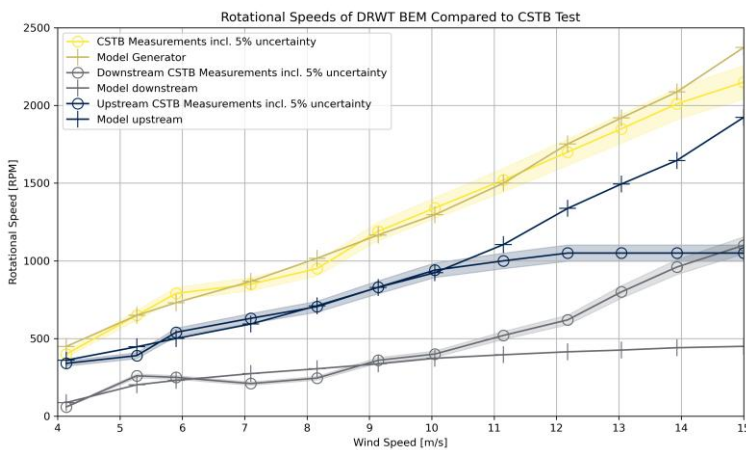


Figure 8: Results of rotational speeds during the wind tunnel test compared to BEM results. The figure shows both rotors individually, the CR-DRWT, and the wind tunnel test data

3.3 Optimization

325 The results of the optimization sweep are presented in Fig. 9. The plot shows the cumulative results of 121 pairs of pitch combinations. The optimization favours the upstream rotor to operate at a high pitch angle and the downstream rotor at a low pitch angle. The best configuration is an upstream rotor at pitch 9° and the downstream rotor at 0° , yielding a possible AEP of 2150 kWh. The results of the extended BEM model with the optimized pitch settings is shown in Fig. 10 and Fig. 11. The maximum aerodynamic power output of the CR-DRWT at 15 m/s is 2251 W with a maximum CP of 0.56 at 14 and 15 m/s.

330 This maximum aerodynamic power is above the rated capacity of 1400 W of the current generator. The corresponding TSR values are calculated using the free stream windspeed for the upstream rotor and the reduced axial velocity for the downstream rotor. The mean TSR values across the wind speed range for the upstream and downstream rotor are 3.2 and 6.6 respectively. Leading to a maximum RPM of the generator at 15 m/s of 1603 RPM, which is significantly below the measured 2150 RPM in the wind tunnel test at the same wind speed. Compared to the wind tunnel tests at CSTB, the optimized CR-DRWT could outperform the current turbine. The current plots shows only aerodynamic performance.

335 However, even including 70-90% electrical losses the optimized turbine outperforms the current measurements. Also, Fig. 11 shows that the optimization maximizes performance of the downstream rotor with a much higher CP for the downstream rotor for all windspeeds compared to the CP for the upstream rotor.

340

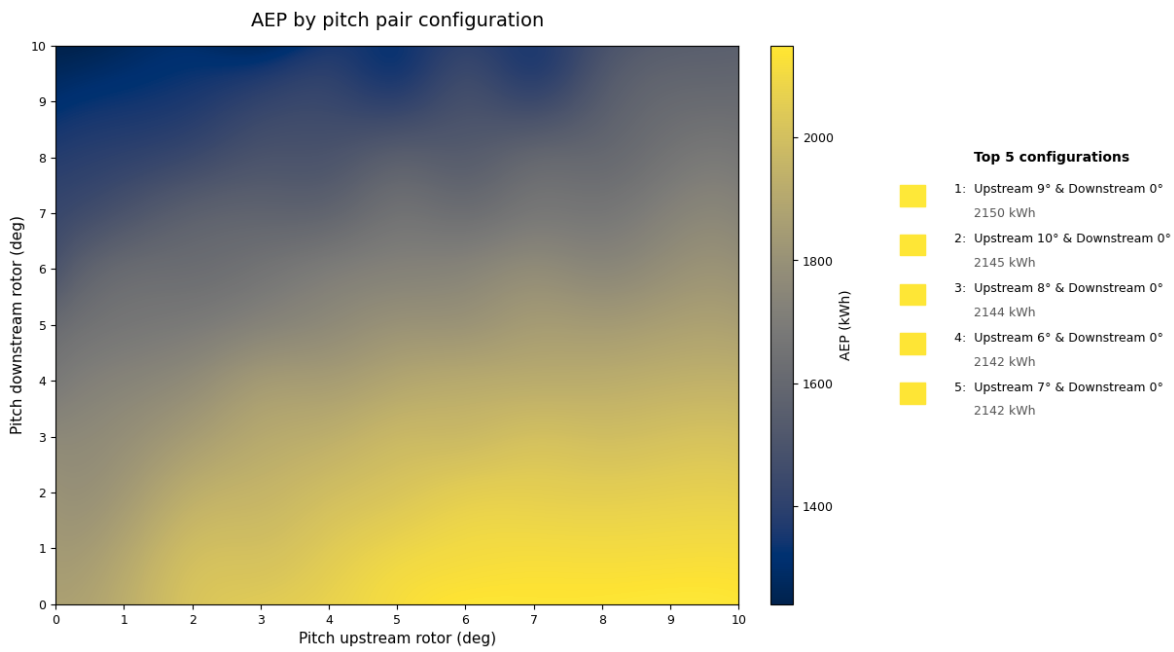


Figure 9: Results of Optimization.

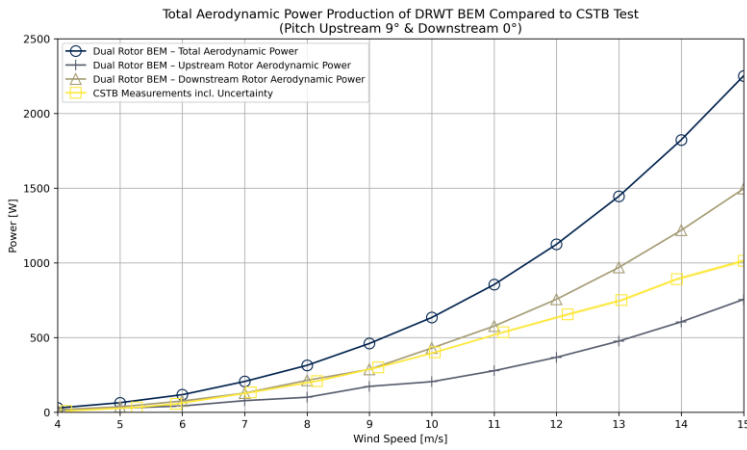
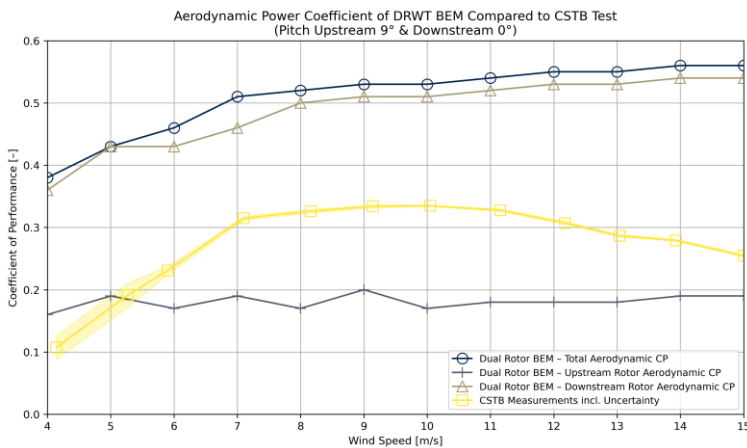


Figure 10: Power production of optimized CR-DRWT.



345 Figure 11: Power coefficient of optimized CR-DRWT.

4 Discussion

The current iteration of the CR-DRWT shows improvement with respect to earlier work (Adema et al., 2025). Especially as precise RPM and pitch measurements are performed. Absolute CP values of around 0.5 are both found in field studies as well as in modelling of CR-DRWT systems (Amoretti et al., 2023; Jung et al., 2005; Koehuan et al., 2017). The current

350 experimental results reach only a maximum CP of 0.33. The findings of this study are more in line with earlier wind tunnel experiments on a CR-DRWT of comparable size (Mitulet et al., 2015; Zhao et al., 2020). There is therefore still potential to increase the efficiency of turbines with limited rotor size. The optimization does show theoretical values reaching a CP of 0.56 confirming the possible improvements.

While the extended BEM model follows the experiments measurements well the deviation between the modelled and measured upstream rotor RPM values above 11 m/s warrants further consideration. The experimental measurements at the upstream rotor plateau at approximately 1050 RPM and the model predicts a continuously increasing RPM to keep torque balance. A possible explanation lies in the measurement system employed during the wind tunnel campaign. The upstream rotor RPM was measured using a light gate sensor reading optical pulses through a slotted disk. It is suspected that a limitation in the pulse counting implementation code effectively imposed an artificial ceiling on the recorded RPM values. This would cause the sensor output to remain at a fixed reading even as the true rotational speed continued to increase. The generator RPM, derived from the generator characteristic curve is therefore considered the more reliable indicator of actual generator RPM. This interpretation is further supported by the fact that the total generator RPM coming from the BEM model matches well with the derived generator RPM.

The theoretical optimization shows the downstream rotor operating with high CP values and limiting the upstream rotor efficiency. This raises questions if a single rotor could achieve better AEP performance than the optimized CR-DRWT. Thereto, the BEM model is run with an isolated upstream rotor effectively modelling single rotor operation and the optimal operation point is found by sweeping across a range of pitch angles and TSR values and maximizing AEP. The optimal aerodynamic performance of a single rotor is found at 0 degrees pitch an a TSR of 6.5. The results are shown in Fig. 10. A single rotor can reach as good as equal power and efficiency. The CR-DRWT has slightly higher AEP with 2322 kWh compared to 2093 for the single rotor. However, the operational point of both systems is different with the CR-DRWT reaching maximum power at 1603 RPM at the generator and 1164 RPM for the single rotor. Highlighting that for both configurations a different generator likely is needed to reach optimal operation. What is worth mentioning is that (Adema et al., 2025) concluded that the current direct drive configuration is not optimized for single rotor operation. The same turbine with 2.5 degrees pitch for the upstream rotor and a stationary downstream rotor only reached a maximum CP in single rotor operation of 0.23. For the current small wind turbine generator the additional costs for a second rotor may be lower than the addition of a gearbox, highlighting the potential of DRWT systems in compact simplified designs (Booker et al., 2010).

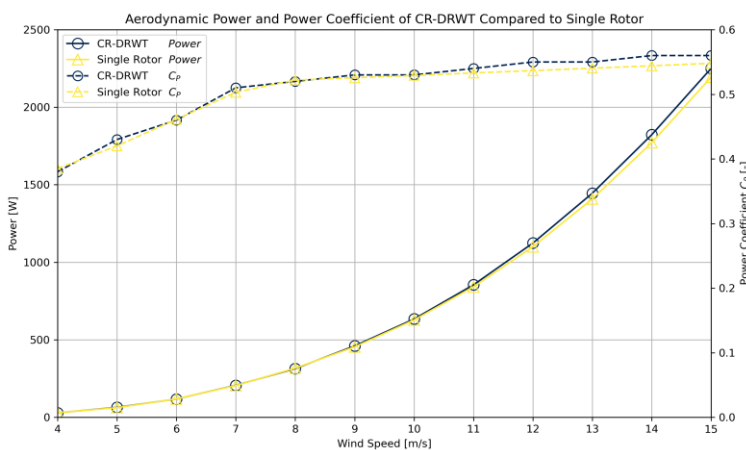


Figure 12: Comparison between theoretical optimal power production and power coefficient of CR-DRWT and Single rotor

380 In most existing wind tunnel experiments, Reynolds numbers are much lower than those encountered in actual situations, limiting their ability to replicate real-world conditions. This limits the ability to model and predict the performance of DRWT's in real-world conditions (Hollands et al., 2020). The same holds for the current experiment with Reynolds numbers

between 25.000 and 200.000. Attention needs to be paid to possible inaccuracies in predicting airfoil characteristics at such low numbers.

385 An attempt to use a BEM model incorporating both axial and tangential influences on the inflow at the downstream rotor (Amoretti et al., 2023), as well as an extension for a dual rotational armature design has shown good agreement with the current findings while some deviations remain. An additional CFD analysis of the current turbine configuration presented in this study will be a valuable addition in understanding the flow field around both rotors. Knowing the detailed flow field around the downstream rotor a detailed aerodynamic design can be performed to further optimize the CR-DRWT. Also, such
390 an analysis may reveal unknown (3 dimensional) aerodynamic effects not captured in current BEM model.

Finally, calculation methods have been proposed for optimizing the downstream rotor geometry for DRWT designs (Bontempo and Manna, 2025; Wang et al., 2018). Currently, for simplicity, the downstream rotor is mirrored with respect to the upstream rotor. Using the BEM model presented in this work a detailed blade design using these design methods can be performed to further increase the performance of dual rotor wind turbines.

395 **5 Conclusions**

This study investigates the performance of a CR-DRWT with dual rotational armature configuration through wind tunnel testing at CSTB in Nantes, France. The research extends previous work by incorporating enhanced measurement capabilities including RPM and pitch angle sensors, the development of an extended BEM model for dual rotational armature systems, and implementing a sweep optimization strategy to identify optimal operating parameters. Wind tunnel tests were conducted
400 at wind speeds ranging from 4 to 15 m/s with a 1.6 m diameter rotor and two rotors with 0.39 D spacing. The CR-DRWT achieved a maximum power output of 1014 W. The extended BEM model is validated against experimental data. The main conclusions are:

- The extended BEM mode for dual rotational armature design showed good overall agreement with wind tunnel measurements for power production, efficiency, and generator RPM and an optimization strategy revealed optimum
405 operational parameters. The upstream rotor RPM measured by the light gate sensor limited at approximately 1050 RPM above 11 m/s, likely due to a pulse counting limitation in the data acquisition code, as the derived generator RPM continued to rise in line with model predictions across the full wind speed range.
- Experimental wind tunnel testing achieved a maximum CP of 0.33, which is higher than previous iterations of the same turbine but below the theoretically optimized value of 0.56, indicating substantial room for improvement
410 through optimal pitch angle, tip-speed ratios for both rotors, and generator choice or redesign.
- The sweep optimization identified an upstream rotor pitch of 9° and downstream rotor pitch of 0° as the optimal configuration for this CR-DRWT with a theoretical AEP of 2150 kWh. The optimization consistently favoured a high-efficiency downstream rotor operating at high CP values while the upstream rotor operates at reduced efficiency, indicating that shared power production across both rotors is essential for maximizing overall system
415 performance.
- The CR-DRWT with dual rotational armature design demonstrated reliable operation with self-starting capability at 3.5 m/s. The dual rotational armature configuration eliminates the need for gearboxes, potentially offering a more cost-effective and mechanically simpler solution for compact small wind turbine designs, particularly suited for urban applications requiring low noise and vibration.

420 To advance the understanding and performance of CR-DRWT systems, detailed computational fluid dynamics simulations should be performed to capture 3D flow effects not modelled by the current BEM approach. Experiments at higher Reynolds numbers closer to real-world operational conditions are needed to improve performance prediction accuracy and validate

airfoil characteristics. The development of blade geometries specifically optimized for the downstream rotor, rather than using mirrored configurations, should be pursued using the validated BEM model and advanced design methods from recent literature. Field testing under real atmospheric conditions is essential to assess practical performance, durability, and economic viability of the optimized CR-DRWT configuration.

Code and data availability

The models and data used in this paper can be requested from the corresponding author upon request.

Author contribution

NA: Conceptualization, Formal Analysis, Writing – Original Draft Preparation. JGV: Investigation, Resources, Writing – Original Draft Preparation. WS: Investigation, Resources, Writing – Review & Editing. AdR: Funding Acquisition, Supervision, Writing – Review & Editing. GS: Writing – Review & Editing

Competing interests

The authors declare that they have no conflict of interest

Acknowledgements

The authors of this paper would like to express their sincere gratitude to Callum Morgan, Sjoerd Kluvers, Wessel Smeenge, Bram Roorda, and Marijn Verbeek, who helped design and build the current iteration of the turbine used in this work, their efforts cannot go unmentioned. Second, the staff at CSTB is thanked for their assistance and guidance during the wind tunnel measurements. Finally, the authors would like to thank Caroline Braud for her effort in facilitating the hosting of the ISWTC at CSTB in 2025.

Financial Support

This work was partially supported by the Nationaal Regieorgaan Praktijkgericht Onderzoek SIA (RAAK.MKB17.007)

References

Adema, N., Swart-Ranshuysen, W., De Ruijter, A., and Schepers, G.: Wind Tunnel Test of Counter-Rotating Dual Rotor Wind Turbine With Double Rotational Armature Design, *Wind Energy*, 28, <https://doi.org/10.1002/we.70039>, 2025.

Al-Obaidi, A. S. M. and Madivaanan, G.: Investigation of the Blockage Correction to Improve the Accuracy of Taylor's Low-Speed Wind Tunnel, *J. Phys.: Conf. Ser.*, 2222, 012008, <https://doi.org/10.1088/1742-6596/2222/1/012008>, 2022.

Amoretti, T., Huet, F., Garambois, P., and Roucoules, L.: Configurable dual rotor wind turbine model based on BEM method: Co-rotating and counter-rotating comparison, *Energy Conversion and Management*, 293, 117461, <https://doi.org/10.1016/j.enconman.2023.117461>, 2023.

QBlade - Next Generation Wind Turbine Simulation: <https://qblade.org/>, last access: 13 April 2026.

Bai, H., Wang, N., and Wan, D.: Numerical study of aerodynamic performance of horizontal axis dual-rotor wind turbine under atmospheric boundary layers, *Ocean Engineering*, 280, 114944, <https://doi.org/10.1016/j.oceaneng.2023.114944>, 2023.

- 455 Bereziartua-Gonzalez, L., Retegi, A., and Ukar, O.: Human-centered integration of small wind turbines in urban environments: a semi-systematic review from an industrial design perspective, *Front. Sustain. Cities*, 7, <https://doi.org/10.3389/frsc.2025.1561894>, 2025.
- Bianchini, A., Bangga, G., Baring-Gould, I., Croce, A., Cruz, J. I., Damiani, R., Erfort, G., Simao Ferreira, C., Infield, D., Nayeri, C. N., Pechlivanoglou, G., Runacres, M., Schepers, G., Summerville, B., Wood, D., and Orrell, A.: Current status and grand challenges for small wind turbine technology, *Wind Energy Science*, 7, 2003–2037, <https://doi.org/10.5194/wes-7-2003-2022>, 2022.
- 460 Bontempo, R. and Manna, M.: Optimum design of contra-rotating wind turbines with adjacent rotors, *Energy Conversion and Management*, 324, 119267, <https://doi.org/10.1016/j.enconman.2024.119267>, 2025.
- Booker, J. D., Mellor, P. H., Wrobel, R., and Drury, D.: A compact, high efficiency contra-rotating generator suitable for wind turbines in the urban environment, *Renewable Energy*, 35, 2027–2033, <https://doi.org/10.1016/j.renene.2010.02.003>, 2010.
- 465 Braud, C., Podvin, B., and Deparday, J.: Study of the wall pressure variations on the stall inception of a thick cambered profile at high Reynolds number, *Phys. Rev. Fluids*, 9, 014605, <https://doi.org/10.1103/PhysRevFluids.9.014605>, 2024.
- Calautit, K. and Johnstone, C.: State-of-the-art review of micro to small-scale wind energy harvesting technologies for building integration, *Energy Conversion and Management: X*, 20, 100457, <https://doi.org/10.1016/j.ecmx.2023.100457>, 2023.
- 470 Chagas, C. C. M., Pereira, M. G., Rosa, L. P., da Silva, N. F., Freitas, M. A. V., and Hunt, J. D.: From Megawatts to Kilowatts: A Review of Small Wind Turbine Applications, *Lessons From The US to Brazil, Sustainability*, 12, 2760, <https://doi.org/10.3390/su12072760>, 2020.
- Chen, T. Y. and Liou, L. R.: Blockage corrections in wind tunnel tests of small horizontal-axis wind turbines, *Experimental Thermal and Fluid Science*, 35, 565–569, <https://doi.org/10.1016/j.expthermflusci.2010.12.005>, 2011.
- 475 Drela, M.: XFOIL: An Analysis and Design System for Low Reynolds Number Airfoils, in: *Low Reynolds Number Aerodynamics*, 1–12, https://doi.org/10.1007/978-3-642-84010-4_1, 1989.
- Erturk, E., Sivrioglu, S., and Bolat, F. C.: Analysis Model of a Small Scale Counter-Rotating Dual Rotor Wind Turbine with Double Rotational Generator Armature, *International Journal of Renewable Energy Research (IJRER)*, 8, 1849–1858, 2018.
- 480 Gur, O.: Extending Blade-Element Model to Contra-Rotating Configuration, *IOP Conf. Ser.: Mater. Sci. Eng.*, 638, 012001, <https://doi.org/10.1088/1757-899X/638/1/012001>, 2019.
- Habash, R. W. Y., Groza, V., Yang, Y., Blouin, C., and Guillemette, P.: Performance of a Contrarotating Small Wind Energy Converter, *International Scholarly Research Notices*, 2011, 828739, <https://doi.org/10.5402/2011/828739>, 2011.
- 485 Hansen, M.: *Aerodynamics of Wind Turbines*, 3rd ed., Routledge, London, 188 pp., <https://doi.org/10.4324/9781315769981>, 2015.
- Hollands, E. O., He, C., and Gan, L.: A particle image velocimetry study of dual-rotor counter-rotating wind turbine near wake, *J Vis*, 23, 425–435, <https://doi.org/10.1007/s12650-020-00643-0>, 2020.
- 490 Jansma, H.: *Development and Optimization of a Generator Test Rig for Small Wind Turbines: Improving Performance and Efficiency*, Hanze UAS, Groningen, 74 pp., 2024.
- Jeong, H., Lee, S., and Kwon, S.-D.: Blockage corrections for wind tunnel tests conducted on a Darrieus wind turbine, *Journal of Wind Engineering and Industrial Aerodynamics*, 179, 229–239, <https://doi.org/10.1016/j.jweia.2018.06.002>, 2018.
- Jung, S. N., No, T.-S., and Ryu, K.-W.: Aerodynamic performance prediction of a 30 kW counter-rotating wind turbine system, *Renewable Energy*, 30, 631–644, <https://doi.org/10.1016/j.renene.2004.07.005>, 2005.
- 495 Jurasz, J., Bochenek, B., Wieczorek, J., Jaczewski, A., Kies, A., and Figurski, M.: Energy potential and economic viability of small-scale wind turbines, *Energy*, 322, 135608, <https://doi.org/10.1016/j.energy.2025.135608>, 2025.
- Koehuan, V. A., Sugiyono, and Kamal, S.: Investigation of Counter-Rotating Wind Turbine Performance using Computational Fluid Dynamics Simulation, *IOP Conf. Ser.: Mater. Sci. Eng.*, 267, 012034, <https://doi.org/10.1088/1757-899X/267/1/012034>, 2017.

- 500 Kutt, F., Blecharz, K., and Karkosiński, D.: Axial-Flux Permanent-Magnet Dual-Rotor Generator for a Counter-Rotating Wind Turbine, *Energies*, 13, 2833, <https://doi.org/10.3390/en13112833>, 2020.
- Lee, S., Kim, H., Son, E., and Lee, S.: Effects of design parameters on aerodynamic performance of a counter-rotating wind turbine, *Renewable Energy*, 42, 140–144, <https://doi.org/10.1016/j.renene.2011.08.046>, 2012.
- 505 Li, Y., Zhang, J., Li, Z., Yang, P., and Wang, H.: Design and verification of a novel double rotor without stator wind turbine generation system, *Energy Reports*, 7, 161–172, <https://doi.org/10.1016/j.egy.2021.10.041>, 2021.
- Mituleț, L.-A., Oprina, G., Chihai, R.-A., Nicolaie, S., Nedelcu, A., and Popescu, M.: Wind Tunnel Testing for a New Experimental Model of Counter-rotating Wind Turbine, *Procedia Engineering*, 100, 1141–1149, <https://doi.org/10.1016/j.proeng.2015.01.477>, 2015.
- 510 Montgomerie, B.: Methods for Root Effects, Tip Effects and Extending the Angle of Attack Range to $\pm 180^\circ$, with Application to Aerodynamics for Blades on Wind Turbines and Propellers, Swedish Defence Research Agency, 2004.
- Mühle, F., Adaramola, M. S., and Sætran, L.: The effect of rotational direction on the wake of a wind turbine rotor – a comparison study of aligned co- and counter rotating turbine arrays, *Energy Procedia*, 137, 238–245, <https://doi.org/10.1016/j.egypro.2017.10.346>, 2017.
- 515 Newman, B. G.: Multiple actuator-disc theory for wind turbines, *Journal of Wind Engineering and Industrial Aerodynamics*, 24, 215–225, [https://doi.org/10.1016/0167-6105\(86\)90023-1](https://doi.org/10.1016/0167-6105(86)90023-1), 1986.
- Ozbay, A., Tian, W., and Hu, H.: An Experimental Investigation on the Aeromechanics and Near Wake Characteristics of Dual-Rotor Wind Turbines (DRWTs), in: 32nd ASME Wind Energy Symposium, American Institute of Aeronautics and Astronautics, <https://doi.org/10.2514/6.2014-1085>, 2014.
- 520 Peng, X., Duan, L., Li, G., Jin, Y., and Han, Z.: Interference between main and auxiliary rotors in floating dual-rotor wind turbines under stationary and surge conditions, *Ocean Engineering*, 322, 120462, <https://doi.org/10.1016/j.oceaneng.2025.120462>, 2025.
- Rosenberg, A., Selvaraj, S., and Sharma, A.: A Novel Dual-Rotor Turbine for Increased Wind Energy Capture, *J. Phys.: Conf. Ser.*, 524, 012078, <https://doi.org/10.1088/1742-6596/524/1/012078>, 2014.
- 525 Schepers, J. G., Adema, N. C., Lipian, M., Kulak, M., Shahid, A., Best, A., Bendre, T., Gallicchio, I., Elsabbagh, A., Mostafa, A., Kim, T., Mikkelsen, R., Gaunaa, M., Teuwen, J. J. E., Rudolf, R. T., Wood, D., and Holierhoek, J. G.: Lessons learned from 10 years of wind tunnel tests on small wind turbines designed by students, *J. Phys.: Conf. Ser.*, 2767, 072009, <https://doi.org/10.1088/1742-6596/2767/7/072009>, 2024.
- Simic, Z., Havelka, J. G., and Bozicevic Vrhovcak, M.: Small wind turbines – A unique segment of the wind power market, *Renewable Energy*, 50, 1027–1036, 2013.
- 530 Sundararaju, H., Lo, K. H., Metcalfe, R., and Wang, S. S.: Aerodynamics and CFD analysis of equal size dual-rotor wind turbine, *Journal of Renewable and Sustainable Energy*, 9, 043305, <https://doi.org/10.1063/1.4999500>, 2017.
- Wang, K., Liu, T., Wan, Y., Ong, M. C., and Wu, T.: Numerical Investigation on Aerodynamic Characteristics of Dual-Rotor Wind Turbines, *Journal of Marine Science and Engineering*, 10, 1887, <https://doi.org/10.3390/jmse10121887>, 2022.
- 535 Wang, Z., Ozbay, A., Tian, W., and Hu, H.: An experimental study on the aerodynamic performances and wake characteristics of an innovative dual-rotor wind turbine, *Energy*, 147, 94–109, <https://doi.org/10.1016/j.energy.2018.01.020>, 2018.
- Yin, F. F., Chen, J. J., Li, X. K., Ye, Z. L., Tang, W., Shen, X., and Guo, X. J.: A blade element momentum model for dual-rotor wind turbines considering inter-rotor velocity interferences, *J. Phys.: Conf. Ser.*, 2265, 042058, <https://doi.org/10.1088/1742-6596/2265/4/042058>, 2022.
- 540 Yuan, W., Tian, W., Ozbay, A., and Hu, H.: An experimental study on the effects of relative rotation direction on the wake interferences among tandem wind turbines, *Sci. China Phys. Mech. Astron.*, 57, 935–949, <https://doi.org/10.1007/s11433-014-5429-x>, 2014.
- Zhao, X., Zhou, P., Liang, X., and Gao, S.: The aerodynamic coupling design and wind tunnel test of contra-rotating wind turbines, *Renewable Energy*, 146, 1–8, <https://doi.org/10.1016/j.renene.2019.06.118>, 2020.